



## Article

# Synthesis and Characterization of Nd:YAG Ceramics for Laser Applications

Olga Alondra Echartea-Reyes <sup>1</sup>, Gloria Verónica Vázquez <sup>2</sup>, José Adalberto Castillo-Robles <sup>1</sup> ,  
Juan López-Hernández <sup>1</sup> , Carlos Adrián Calles-Arriaga <sup>1</sup> , Wilian Jesús Pech-Rodríguez <sup>1</sup>   
and Enrique Rocha-Rangel <sup>1,\*</sup> 

<sup>1</sup> Research and Graduate Department, Universidad Politécnica de Victoria, Ciudad Victoria 87138, Mexico; ochartear@upv.edu.mx (O.A.E.-R.); jcastillor@upv.edu.mx (J.A.C.-R.); jllopezh@upv.edu.mx (J.L.-H.); ccallesa@upv.edu.mx (C.A.C.-A.); wpechr@upv.edu.mx (W.J.P.-R.)

<sup>2</sup> Laboratorio de Óptica Integrada, Centro de Investigaciones en Óptica, A. C., León 37150, Mexico; gvvazquez@cio.mx

\* Correspondence: erochar@upv.edu.mx; Tel.: +52-834-171-1100

**Abstract:** Materials known as Nd:YAG are crystalline materials of the cubic system made from the neodymium-doped yttrium aluminum garnet, which, among others, have excellent optical properties. Nd:YAG four-level laser devices are frequently used in both the health and industrial sectors. In this study, a simple and inexpensive alternative to manufacturing Nd:YAG materials through solid state reactions following powder processing routes was proposed. For this, an intense mixture of the precursor materials ( $\text{Al}_2\text{O}_3$  and  $\text{Y}_2\text{O}_3$ ) was carried out, followed by the addition of neodymium atoms to improve the optical properties of the resulting material. High-energy mechanical mixing of the precursor powders resulted in submicron particles with good size distributions of the powders. The advance of YAG formation was monitored by intermediate phase formation during heat treatment through interrupted tests at different temperatures and analysis by X-ray diffraction. From this analysis, it was found that reaction for the formation of the desired YAG is completed at 1500 °C. Fourier transform infrared spectroscopy analyses determined the presence of functional groups corresponding to the YAG. Finally, the study employing optical emission spectroscopy showed wavelengths in agreement with those of the electronic structure of the elements of the synthesized Nd:YAG.

**Keywords:** Nd-YAG; laser; optical characterization



**Citation:** Echartea-Reyes, O.A.; Vázquez, G.V.; Castillo-Robles, J.A.; López-Hernández, J.; Calles-Arriaga, C.A.; Pech-Rodríguez, W.J.; Rocha-Rangel, E. Synthesis and Characterization of Nd:YAG Ceramics for Laser Applications. *Ceramics* **2023**, *6*, 1655–1666. <https://doi.org/10.3390/ceramics6030102>

Academic Editor: Antonio Riveiro

Received: 13 May 2023

Revised: 4 June 2023

Accepted: 14 June 2023

Published: 2 August 2023



**Copyright:** © 2023 by the authors. Licensee MDPI, Basel, Switzerland. This article is an open access article distributed under the terms and conditions of the Creative Commons Attribution (CC BY) license (<https://creativecommons.org/licenses/by/4.0/>).

## 1. Introduction

Materials known as neodymium-doped yttrium aluminum garnet (Nd:YAG) are crystalline materials of the cubic system made from neodymium-doped yttrium aluminum garnet. These materials have excellent physical, chemical, thermal, mechanical, and optical properties [1–7]. One of the applications of this type of material is its widespread use in white-light emitter manufacturing. However, the development of lasers has always been conditioned by the availability of suitable materials for their use. In 1995, Ikesue et al. demonstrated that transparent Nd:YAG ceramics could be produced using ceramic fabrication techniques such as dry pressing and sintering [2]. Therefore, sintering of active media by ceramic methods has become an alternative for solid-state laser active media manufacturing. The addition of dopants during the processing of ceramic materials favors the generation of concentration gradients that successfully modify the characteristics of the materials [3].

There are different synthesis routes for Nd:YAG, including the solid-state reaction, the solvothermal synthesis and a lot of wet chemical methods. As an example, the Nd-YAG has been synthesized by means of Colloidal suspension of primary oxides (i.e.,  $\text{Y}_2\text{O}_3$ ,

$\text{Al}_2\text{O}_3$ ,  $\text{Nd}_2\text{O}_3$ , and  $\text{SiO}_2$ ) used as sintering aid and posterior sintered by vacuum sintering, followed by post-sintering treatment by Hot Isostatic Pressing (HIP) [8]; by the slip casting method of a slurry prepared with the  $\text{Al}_2\text{O}_3$  and  $\text{Y}_2\text{O}_3$  commercial powders and a series of organics additives [9]; from a bulk crystal using femtosecond laser-induced preferential etching [10].  $\text{YAG}:\text{Ce}^{3+}$  phosphor was also prepared by a series of amine-assisted co-precipitation methods [11]. In addition, the fabrication of highly-doped  $\text{Nd}^{3+}:\text{YAG}$  transparent by reactive SPS has been reported [12]. Finally,  $\text{Al}_2\text{O}_3\text{-Ce}:\text{YAG}$  and  $\text{Al}_2\text{O}_3\text{-Ce}:(\text{Y,Gd})\text{AG}$  composite ceramic phosphors were produced by reactive vacuum sintering [13]. The  $\text{Nd}:\text{YAG}$  phosphor obtained by all these methods presents similar properties to the commercial lasers. However, there exists a major drawback, namely that all these methodologies are costly, difficult to implement and not very productive. Therefore, the synthesis of YAG by means of solid-state reactions is of interest due to the simplicity and low cost of this process.

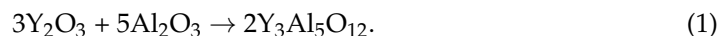
In optical applications such as lasers, it is suggested that the materials to be worked with must have a series of characteristics such as homogeneity, i.e., the absence of second phases with different refractive indexes, and isotropy; the main limitation of ceramic materials is related to the scattering of light due to residual porosity [14]. Chemical structures, compositions, and crystalline contents influence the transparency of ceramic materials. It has been shown that the transparency and therefore laser efficiency are rapidly reduced with the presence of pores [15]. This is the reason that has prompted the development of transparent optical materials focusing on materials with a cubic structure.

Technological advances in the synthesis, shaping, and sintering of ceramic powders have made it possible to adapt the microstructural, mechanical, and optical property relationships in the case of this type of materials [16]. Emphasizing the optical properties, the general condition sought in improving them is their homogeneity with respect to their dielectric properties through solid-state sintering. In order to optimize the reactive solid-state sintering process, Vorona et al. studied the phase composition, microstructure and optical properties of YAG ceramics doped with  $0 \div 0.15\%$  by weight of  $\text{MgO}$ ; after analyzing the characteristics of  $\text{Mg}^{2+}$  ions, the authors concluded that the optimal concentration range of  $\text{MgO}$  sintering contributes to achieving transparent YAG ceramics [17]. Along the same line of research, Wentao Jia studied the quantitative relationship between microstructure and mechanical and optical properties in transparent  $\text{Nd}:\text{YAG}$  ceramics. In his study, W. Jia applied stereology and fractals to identify the quantitative relationship between them and mechanical properties of transparent  $\text{Nd}:\text{YAG}$  ceramics sintered at  $1750^\circ\text{C}$  for 8–50 h [18]. The improvement of laser performance in transparent  $\text{Nd}:\text{YAG}$  ceramics has been investigated by Yuelong Fu, et al. with preparations of 2%  $\text{Nd}:\text{YAG}$  ceramics using a solid-state reactive sintering method [13]. The sintered samples were annealed at different temperatures for different times, obtaining ceramics with high density and homogeneous structure with an average grain size of  $15\ \mu\text{m}$ . They concluded that at  $1450^\circ\text{C}$  and 5 h of retention, the concentration of color centers in the sample is relatively low and the efficiency of the laser slope is the highest.

In addition to the study of the different types of properties and the way they are linked to each other and how they end up affecting the performance of lasers due to their optical properties, there are authors who pay special attention to the behavior and nature of carbon contaminations in their studies, dispersed in the matrix of yttrium aluminum garnet. Kosyanov et al., showed that an increase in applied pressure from 30 to 70 MPa changed the color of the ceramic; the samples darkened and became dark brown, affecting the optical properties of the material [19,20]. To the best of our knowledge, there is no genuine interest in developing improvements in the optical properties by starting from the solid-state sintering of powders and emphasizing the economic and methodological advantages that this type of treatment presents, so the work to be conducted is promising in this area. In addition, the grinding parameters are usually not as long as those previously mentioned, so that the grinding time represents another advantage for its realization.

## 2. Materials and Methods

For the present study, the  $Y_3Al_5O_{12}$  perovskite was synthesized. For this purpose, a mixture in stoichiometric amounts according to Reaction 1 was prepared.



Powders of  $Y_2O_3$  and  $Al_2O_3$  (Sigma-Aldrich, St. Louis, MO, USA, 99.9% purity and 1  $\mu\text{m}$  size) were ground in a planetary mill (Retsch PM 100, Duesseldorf, Germany) for 3 h at a rotation speed of 300 rpm. In addition, a stainless steel container with zirconia grinding elements, 0.3 cm in diameter, was utilized, as well as a powder weight/ball weight ratio of 1:12. After milling, the particle size distribution and specific surface area were determined using the Mastersizer 2000 equipment of English origin. This equipment uses the technique of laser diffraction to measure the particle size and particle size distribution of materials. It achieves this by measuring the intensity of light scattered as a laser beam passes through a dispersed particulate sample. The powder mixtures resulting from the milling step were subjected to thermal treatment at 900, 1100, 1300, and 1500  $^{\circ}\text{C}$  in order to follow the advance of Reaction 1. Thermal treatment was carried out in an electric resistance furnace (Carbolite RHF17/3E, Manchester, UK) for 1 h; the heating speed was 25  $^{\circ}\text{C}/\text{min}$ . To avoid oxidation of the neodymium, a nitrogen atmosphere was used inside the furnace chamber. The advance of the chemical reaction was followed by X-ray diffraction analysis (Siemens, D-5000, Munich, Germany). Once the formation temperature of compound  $Y_3Al_5O_{12}$  was determined (Reaction 1 complete), mixtures were prepared with the two initial components with additions of neodymium (0, 0.25, 0.5 and 1 atomic %). These mixtures were carried out in the planetary mill; the powders were mixed under the same conditions mentioned at the beginning of this methodology. With the powders resulting from the second grinding stage, cylindrical tablets, 1 cm in diameter and 0.3 cm thickness, were obtained by uniaxial compaction at 250 MPa using a press (Porter-30T, México City, Mexico). They were then subjected to sintering treatments for 2 h at 1500  $^{\circ}\text{C}$  in an electric furnace. The density of the sintered samples was evaluated through the Archimedean principle using the standards established in the ASTM C20-00 standard [21]. To determine the functional groups present in the formed compound, FTIR analysis was performed (Rayleigh WQF-510A, Beijing, China). The pump source used to obtain the emission spectra was a laser diode that operated at 806 nm with an optical power of 80 mW; the laser light was collimated by a microscope objective of 10 $\times$ . The absorption spectra of the pills were measured using a Cary 5000 UV-Vis-NIR spectrophotometer, in which the sample was placed so that the waveguides were perpendicular to the incident light beam and a range of 300–900 nm so that it could cover the main absorption bands of the material. Finally, observations of microstructure of sintered samples were performed by optical microscopy (Nikon Eclipse Ma200, Tokyo, Japan).

## 3. Results

### 3.1. Density

Figure 1 shows the apparent density achieved by the sintered samples as a function of the Nd content. What is shown in this figure is that as the Nd content increases, the density of the samples tends to decrease. This is probably because the melting point of Nd is 1024  $^{\circ}\text{C}$ . If the samples were sintered at 1500  $^{\circ}\text{C}$ , the Nd at that temperature must have been in liquid phase and, due to its low wettability, could not move within the mixture to occupy the porosity of the mixture which caused the porosity not to close during sintering. The final density of all samples is relatively low due to the fact that Nd-YAG has density values of approximately 4.5  $\text{gr}/\text{cm}^3$ . It is considered that better densities were not achieved during processing due to the following cause: during heating for sintering, two phenomena occurred that are significantly contradictory. The first one was the diffusion of atoms to achieve the consolidation of the samples. The second one was the occurrence of Reaction 1 for the formation of YAG garnet. The controlling stage of the process was the atomic

diffusion stage which was not high enough to achieve a better densification of the samples. This could be corrected by increasing the sintering temperature to favor atom mobility.

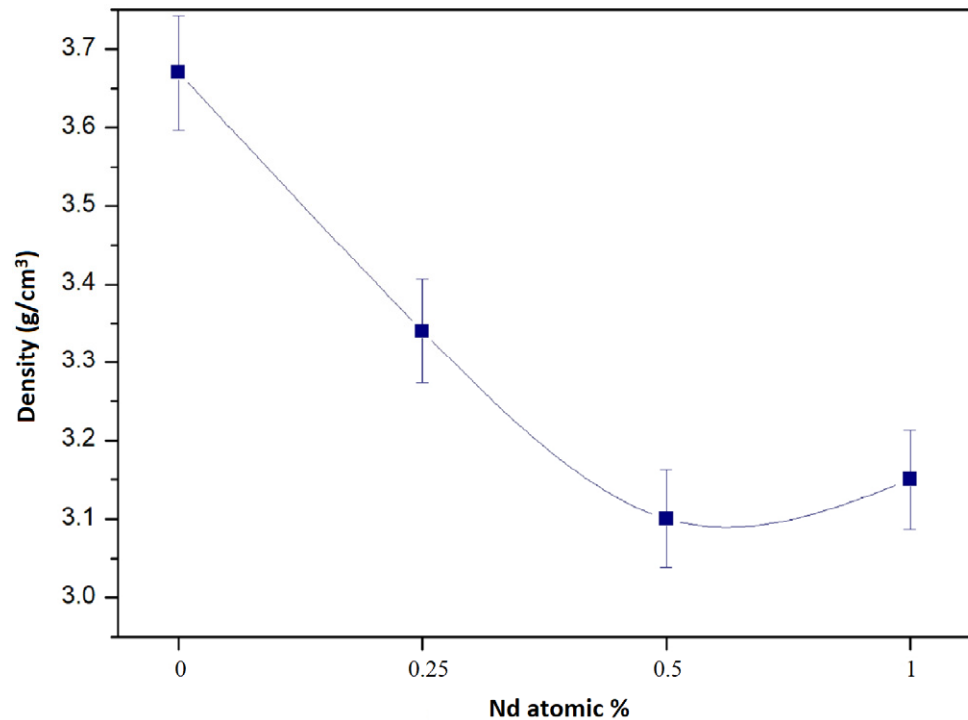


**Figure 1.** Apparent density of sintered  $Y_3Al_5O_{12}$  as a function of the Nd content in it.

### 3.2. Particle Size

Figure 2 shows the results of the particle size distribution analysis for each of the study samples. The figure shows that the particle sizes vary from less than 1 micron to several microns; the sample with a 0.5 at. % Nd exhibits the largest size distribution, with sizes ranging from 0.2 microns to 9 microns. On the other hand, the sample with 1 at. %Nd is the one with the smallest size distribution, since the particle sizes range between 0.2 and 2.5 microns. The sample with 0.25 at. % Nd also shows sizes below 1 micron and maximum sizes of approximately five microns. In comparison, the sample without Nd addition presents sizes between two and five microns. The strong size variation, especially due to the large particle sizes in the sample with a 0.5 at. %Nd, is what causes the densification in this sample to be not so good since during the compaction of the powders in this sample there must have been empty spaces (pores) difficult to close with sintering. According to these results, the samples without Nd and with low Nd content (0.25% Nd) are the ones that densified better. Therefore, the size distribution of these samples is the one that favors the porosity closure during sintering. As mentioned before, the presence of Nd hinders the sintering of the compounds due to the liquid state in which it is present at the temperature (1500 °C) of formation of the compound ( $Y_3Al_5O_{12}$ ), which corresponds to the sintering temperature. During sample consolidation, there are two desirable factors, one is the small size of the powder so that diffusion can occur without problem because atoms can only move across small distances. The other desirable phenomenon is a multimodal particle distribution, i.e., a good variety of sizes, because this favors the increase in the number of contacts between particles and thus the diffusion of atoms and consequent consolidation of the sample. In the case of the sample with a 1% Nd, although the particle size is small, the size distribution is low, which causes this sample not to consolidate properly.

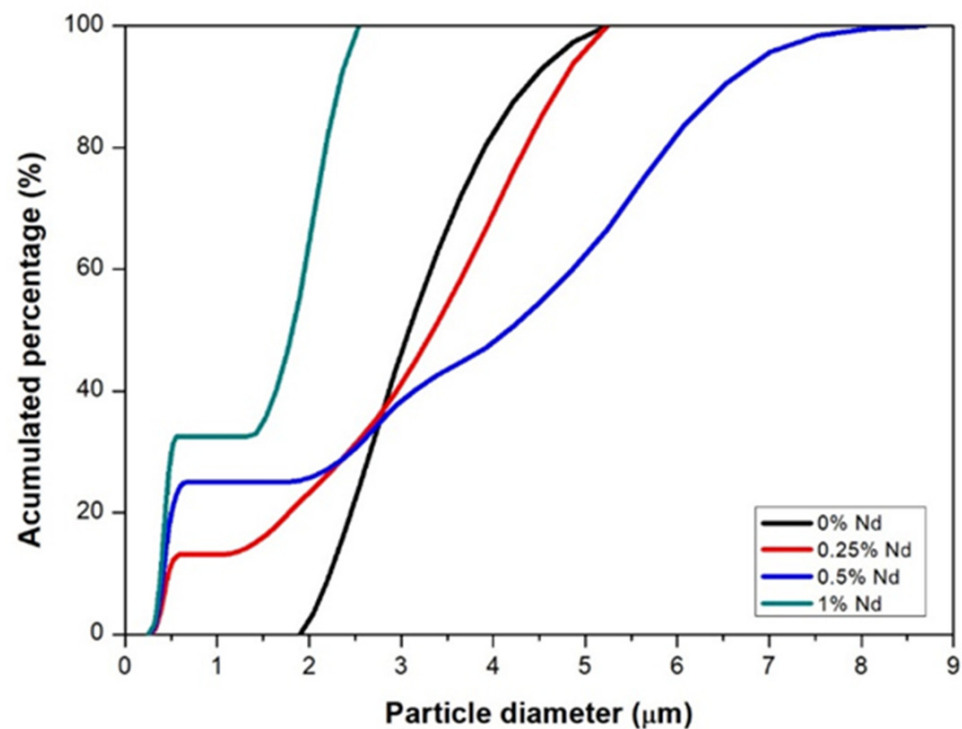


**Figure 2.** Particle size distribution of ground powders with different neodymium additions.

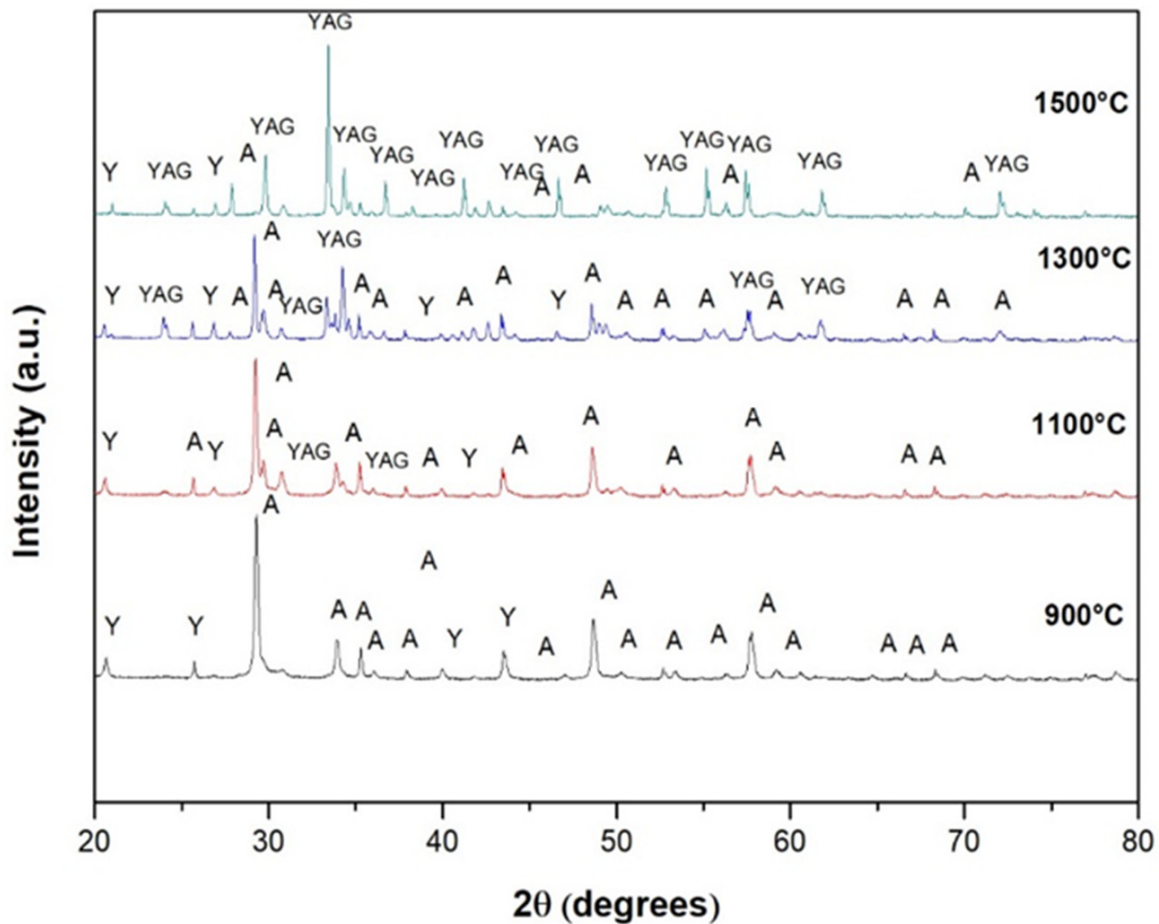
### 3.3. Crystalline Structure

Figure 3 shows the diffraction patterns of the  $Y_2O_3 + Al_2O_3$  powder mixture that was subjected to interrupted tests at different temperatures to observe the progress of reaction 1 and to determine the formation of the  $Y_3Al_5O_{12}$  compound. In this figure, it can be seen that at 900 °C, Reaction 1 did not start. This can be affirmed because the crystalline phases present here correspond to the two original components of sample  $Y_2O_3 + Al_2O_3$ . At 1100 °C, the first traces of the desired garnet formation begin to appear, becoming more abundant at 1300 °C. At 1500 °C, the predominant crystalline phase in the sample corresponds to that of yttrium aluminum garnet ( $Y_3Al_5O_{12}$ ), although some traces of the alumina phase are still observed in the corresponding spectrum. The minimal width of the peaks and their intensity indicate the strong crystallinity of the compound formed. From these spectra, it can be summarized that Reaction 1 starts to occur at approximately 1100 °C and is almost completed at 1500 °C. To eliminate the remaining traces of alumina and yttria at 1500 °C, the samples could be sintered at a higher temperature, e.g., 1550 or 1600 °C.

Diffractions in the resulting spectrum at 1500 °C correspond to Nd-YAG in agreement with JCPDS 79-1892. The unit cell of Nd-YAG was calculated by the least squares method using all reflections of Nd-YAG in the spectrum at 1500 °C of Figure 3. The calculated result reveals that the crystals have a body-centered cubic crystalline structure with space group Ia3d. The lattice parameters for YAG with different additions of Nd are presented in Table 1.

**Table 1.** Lattice parameters of the Nd:YAG crystalline cubic structure as a function of Nd in the composition.

| Nd Atomic % | Lattice Parameter |
|-------------|-------------------|
| 0           | 11.9604           |
| 0.25        | 11.9712           |
| 0.5         | 11.9771           |
| 1           | 11.9814           |



**Figure 3.** Diffraction patterns of the powder mixture  $Y_2O_3 + Al_2O_3$  subjected to interrupted tests at different temperatures to determine the formation temperature of yttrium aluminum garnet ( $Y_3Al_5O_{12}$ ).

The lattice parameter values increase with increasing neodymium in the  $Y_3Al_5O_{12}$  compound due to the slightly larger atomic radius of neodymium (1.82 Å) with respect to yttrium (1.80 Å). However, these values are similar to those reported in the literature [7,22,23].

### 3.4. Fourier Transform Infrared Spectroscopy

Figure 4 shows the absorbance spectrum obtained by Fourier transform infrared spectroscopy of the sample sintered at 1500 °C. This spectrum shows two peaks at 591 and 1034  $cm^{-1}$  which have been associated with the Al-O functional group of alumina. On the other hand, at wavenumbers of 1411 and 1510  $cm^{-1}$ , two other peaks were observed, corresponding to the Y-O functional group matching the yttria. Finally, at 3300  $cm^{-1}$ , one more peak was observed, which was associated with the H-O bond corresponding to water. The presence of this chemical bond is explained by the absorption of water by the sample after it was sintered. From this spectrum, it can be confirmed that the functional groups composing the mixture are those corresponding to the elements of compound  $Y_3Al_5O_{12}$ .

### 3.5. Absorption Spectrum

Absorption studies were performed for the samples with additions of Nd in atomic percentages of 0.25%, 0.5% and 1%. Figure 5 shows the comparative absorption spectra for each of the samples. Predominant absorption bands can be better observed from the 1% Nd sample at around 750 and 810 nm, corresponding to transitions from the  $^4I_{9/2}$  ground level to  $^4F_{7/2}$ : $^4S_{3/2}$  and  $^4F_{5/2}$ : $^4H_{9/2}$  levels, respectively. In addition, peaks at 520, 590 and 880 nm are also present. It can be seen that the bandwidth and the peak shape are the same

for the samples with neodymium content; however, as the concentration increases, the peak absorbance becomes greater.

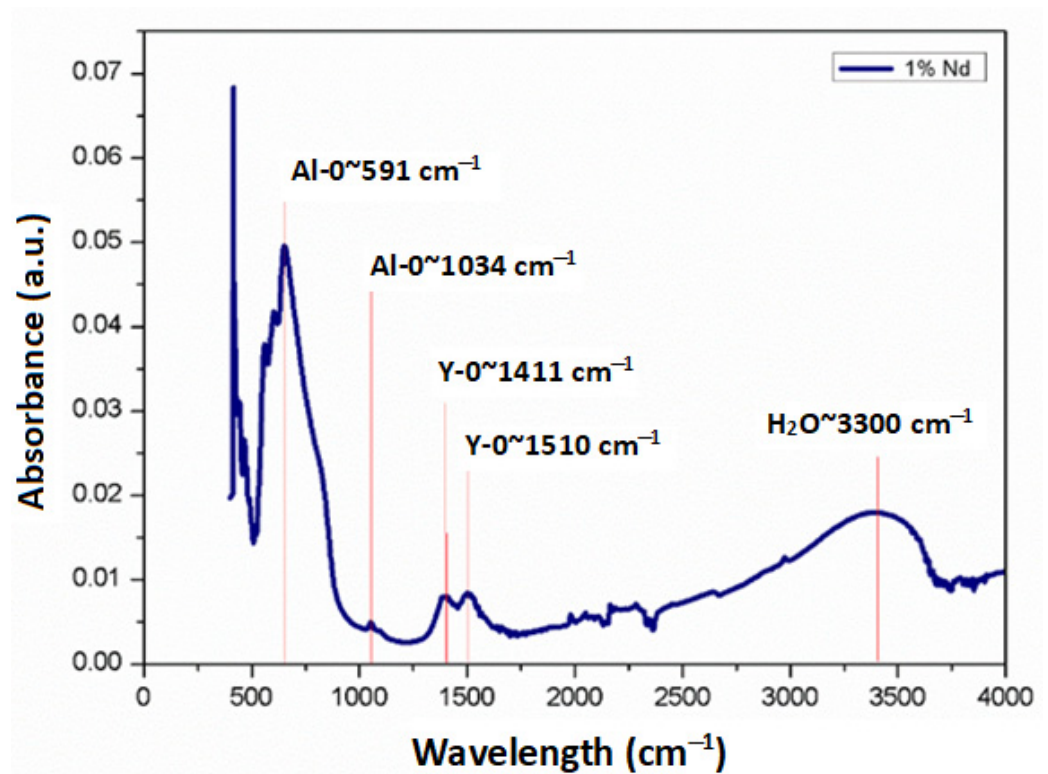


Figure 4. FTIR spectrum obtained from the sample sintered at 1500 °C with addition of 1 at. %Nd.

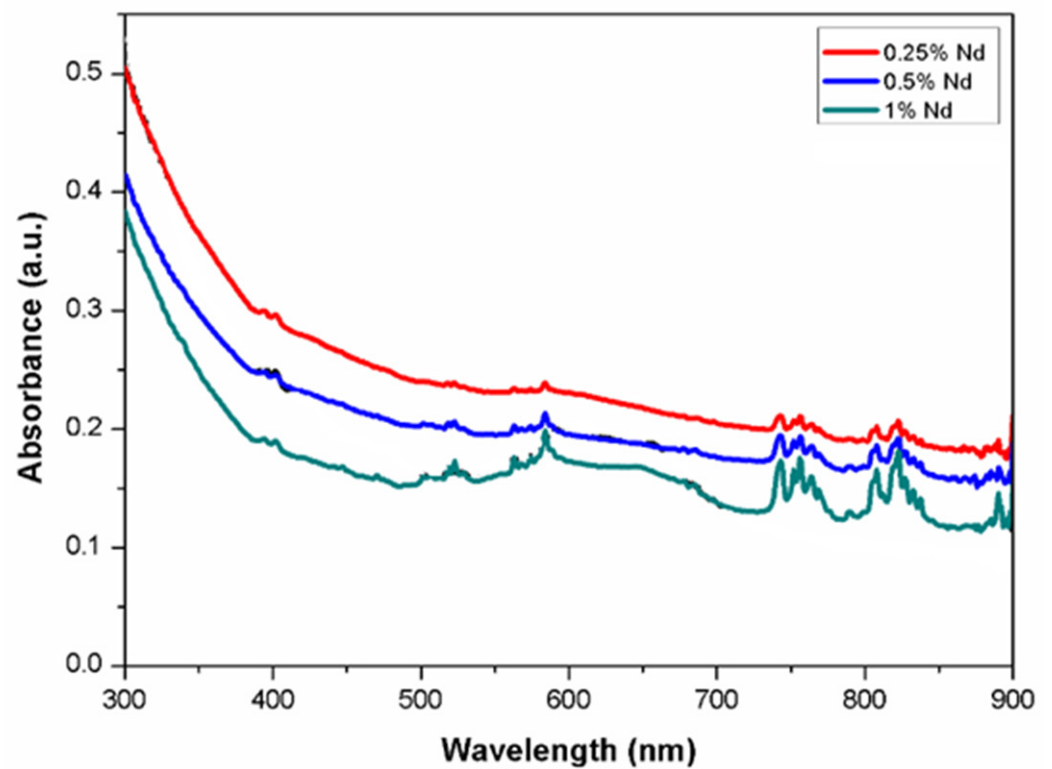
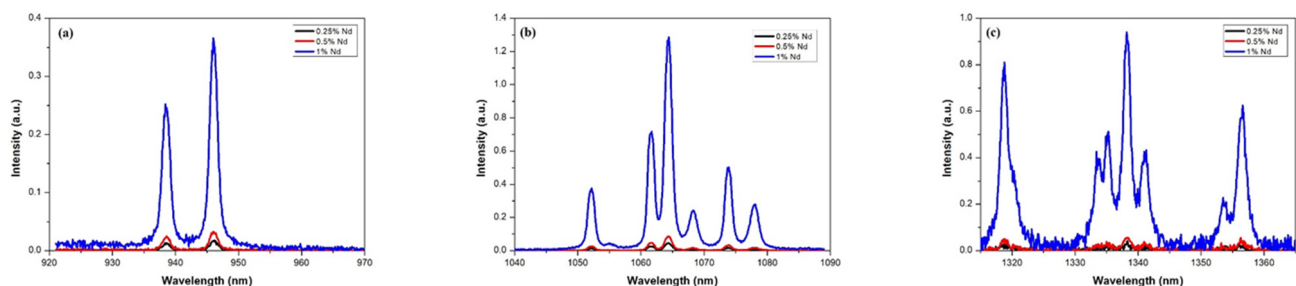


Figure 5. Absorption spectra of Nd in YAG.

### 3.6. Emission Spectrum

Emission studies were carried out at wavelengths from 930 to 1370 nm for the three samples doped with Nd. Figure 6 shows the comparative emission spectra for each of the samples. As can be seen, the peak intensity increases as neodymium concentration increases. Still, the shape of the peaks and the bandwidth are maintained in all cases, which is important in laser emission applications. The emission spectra are presented in the three predominant regions due to radiative decay from the  ${}^4F_{3/2}$  state to the  ${}^4I_{9/2}$ ,  ${}^4I_{11/2}$  and  ${}^4I_{13/2}$  states, which can be seen in the figure. The energy levels of Nd:YAG are determined by the neodymium (Nd) ions in the YAG; the predominant radiative transition at 1064 nm occurs between the upper stark level of the  ${}^4F_{3/2}$  state and one of the  ${}^4I_{11/2}$  states. The synthesized materials could have potential application in the development of a laser that emits in the near infrared region. As depicted in Figure 6, the spectrum shows a broad emission range that could be used for tunable lasers. For example, Okhaphkin et al. [24] reported a tunable Nd:YAG laser with an operating range between 945 and 946 nm. In comparison, Figure 6a shows that at the  $4F_{3/2}$  to  $4I_{9/2}$  transition, two emissions could be utilized in laser tuning from 937 to 939 nm and from 946 to 948 nm. The primary emission shown in Figure 6b corresponding to 1064 nm could be used in double frequency lasers at 532 nm for medical procedures [25,26]. In addition, other emissions observed in the same transition with corresponding peaks ranging from 1052 to 1078 nm could be used for similar purposes. Regarding the third transition from  $4F_{3/2}$  to  $4I_{13/2}$  shown in Figure 6c, the emission peaks are similar to laser wavelengths reported recently by Zhu et al. [27] but with the advantage of an additional emission at 1336 nm.



**Figure 6.** Emission spectra of Nd:YAG for (a) transition  ${}^4F_{3/2} \rightarrow {}^4I_{9/2}$ , (b) transition  ${}^4F_{3/2} \rightarrow {}^4I_{11/2}$  and (c) transition  ${}^4F_{3/2} \rightarrow {}^4I_{13/2}$ .

The values in the luminescent properties, particularly the optical-to-optical, of output laser energy at 1064 nm of the Nd:YAG obtained in this work are similar to both those of the commercial lasers and the lasers obtained by the different methodologies mentioned in the introduction section of this work.

### 3.7. Microstructure

The microstructures of synthesized Nd:YAG obtained from the optical microscope are shown in Figure 7. In general, the microstructure is very fine, made up of irregular grains of different sizes and morphologies (angular, rounded, etc.). Due to the fine microstructure, the porosity of the samples cannot be distinguished. In fact, finer particles are obtained for intermediate Nd contents (0.25 at. % and 0.5 at. %). However, the sample with a 0.5 at. % Nd cracked. According to density measurements, the higher the amount of Nd in the garnet, the lower the bulk density, a situation difficult to observe in these images. However, the very fine size present in these composites due to the type of processing carried out to manufacture them positively influences the optical properties of the composites, as already observed above. This suggests that if the processing conditions of these composites can be better controlled to obtain denser bodies, the optical properties will be further improved.



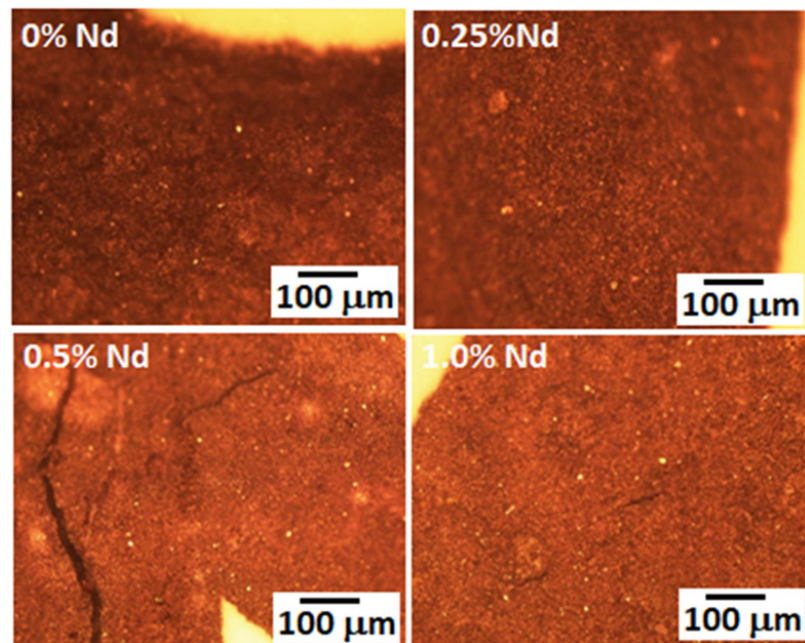


**Figure 7.** Microstructures of different synthesized Nd:YAG, taken from the optical microscope.

The general microstructure of sintered Nd:YAG samples observed with scanning electron microscopy (SEM) is depicted in Figure 8a–d. In these pictures, it is possible to observe that the microstructure in all samples is composed of irregular grains of varied sizes and particle shapes. The samples exhibited a wide distribution of particle sizes with a multimodal behavior. Their micro-structure is composed of larger grains with different contrasts (brighter zones) and various morphological features. These bright grains with different neodymium concentrations are associated with compounds formed during the YAG processing, as detected by SEM-EDS (Figure 9).

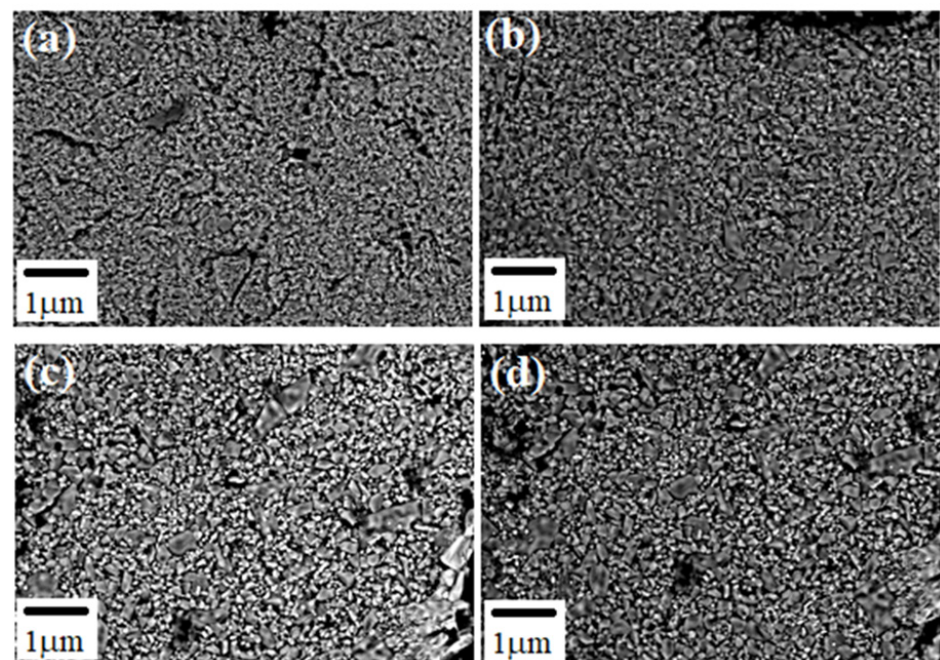


**Figure 8.** Microstructures of different synthesized Nd:YAG, obtained from SEM (a) 0 %Nd, (b) 0.25 %Nd, (c) 0.5 %Nd and (d) 1.0 %Nd.

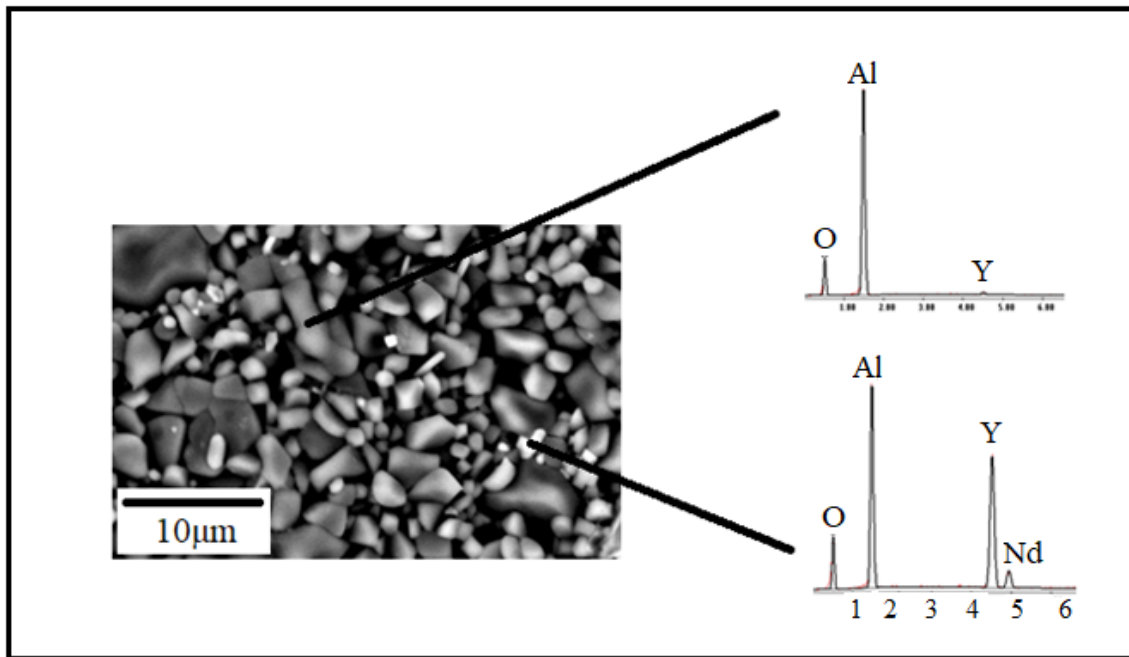


**Figure 9.** EDS analysis performed in the YAG-3% at Nd sintered sample.

#### 4. Conclusions

Through intense mixing of the  $\text{Al}_2\text{O}_3$  and  $\text{Y}_2\text{O}_3$  ceramics in a high-energy mill and subsequent heat treatment at elevated temperature to induce solid-state chemical reactions between the two initial components, the synthesis of the  $\text{Y}_3\text{Al}_5\text{O}_{12}$  compound doped with different percentages of neodymium was feasible. From the characterizations performed on the obtained products, the following results were recorded: X-ray diffraction patterns indicate that the formation of the  $\text{Y}_3\text{Al}_5\text{O}_{12}$  compound by solid-state reaction starts at approximately  $1100^\circ\text{C}$  and is completed at  $1500^\circ\text{C}$ ; likewise, the newly formed compound has a cubic crystalline structure. The spectra obtained by Fourier transform infrared spectroscopy show the presence of the two functional groups (Al-O and Y-O) of the  $\text{Y}_3\text{Al}_5\text{O}_{12}$  compound. The analysis by optical absorption and emission spectroscopy indicates wavelength bands in agreement with the electronic structure of Nd ions in YAG. The microstructure of the manufactured composite is very fine, presenting equiaxed grains with sizes of less than one micron. This explains the good optical characteristics of the manufactured compound. The results are promising for the development of a light source based on a ceramic material obtained by the solid-state reaction method.

**Author Contributions:** Conceptualization, G.V.V., E.R.-R. and C.A.C.-A.; methodology, O.A.E.-R., J.A.C.-R. and J.L.-H.; validation, J.A.C.-R., J.L.-H. and W.J.P.-R.; formal analysis, O.A.E.-R., G.V.V., E.R.-R. and C.A.C.-A.; investigation, O.A.E.-R., J.A.C.-R. and J.L.-H.; resources, G.V.V., J.A.C.-R., J.L.-H., C.A.C.-A., W.J.P.-R. and E.R.-R.; data curation, O.A.E.-R., G.V.V., J.A.C.-R., J.L.-H. and J.A.C.-R.; writing—original draft preparation, O.A.E.-R., G.V.V., C.A.C.-A. and E.R.-R.; writing—review and editing, G.V.V. and C.A.C.-A.; visualization, G.V.V., C.A.C.-A. and E.R.-R.; supervision, G.V.V., C.A.C.-A. and E.R.-R.; project administration, E.R.-R. All authors have read and agreed to the published version of the manuscript.

**Funding:** This research received no external funding.

**Institutional Review Board Statement:** The study does not require ethical approval.

**Informed Consent Statement:** Not applicable.

**Data Availability Statement:** Not applicable.

**Acknowledgments:** OAER thanks the national council of science and technology for the scholarship granted for the completion of her master's studies. all authors agree with this acknowledgement.

**Conflicts of Interest:** The authors declare no conflict of interest.

## References

1. Nakai, S.; Mima, K. Laser driven inertial fusion energy: Present and prospective. *Rep. Prog. Phys.* **2004**, *67*, 321–349. [[CrossRef](#)]
2. Ikesue, A.; Aung, Y.L.; Taira, T.; Kamimura, T.; Yoshida, K.; Messing, G.L. Progress in ceramic lasers. *Annu. Rev. Mater. Res.* **2006**, *36*, 397–429. [[CrossRef](#)]
3. Ikesue, A.; Aung, Y.L. Ceramic laser materials. *Nat. Photon.* **2008**, *2*, 721–727. [[CrossRef](#)]
4. Li, C.-Q.; Zuo, H.-B.; Zhang, M.-F.; Han, J.-C.; Meng, S.-H. Fabrication of transparent YAG ceramics by traditional solid-state-reaction method. *Trans. Nonferrous Met. Soc. China* **2007**, *17*, 148–153. [[CrossRef](#)]
5. Park, J.; Joo, J.; Kwon, S.G.; Jang, Y.; Hyeon, T. Synthesis of Monodisperse Spherical Nanocrystals. *Angew. Chem. Int. Ed.* **2007**, *46*, 4630–4660. [[CrossRef](#)]
6. Boulesteix, R.; Maître, A.; Baumard, J.-F.; Sallé, C.; Rabinovitch, Y. Mechanism of the liquid-phase sintering for Nd:YAG ceramics. *Opt. Mater.* **2009**, *31*, 711–715. [[CrossRef](#)]
7. Kostić, S.; Lazarević, Z.; Radojević, V.; Milutinović, A.; Romčević, M.; Romčević, N.; Valčić, A. Study of structural and optical properties of YAG and Nd:YAG single crystals. *Mater. Res. Bull.* **2015**, *63*, 80–87. [[CrossRef](#)]
8. Jing, W.; Li, F.; Yu, S.; Ji, X.; Xu, T.; Zhang, J.; Pan, Z.; Yuan, Z.; Kang, B.; Deng, J.; et al. High efficiency synthesis of Nd:YAG powder by a spray co-precipitation method for transparent ceramics. *J. Eur. Ceram. Soc.* **2018**, *38*, 2454–2461. [[CrossRef](#)]
9. Mohammadi, F.; Mirzaee, O.; Tajally, M. Influence of solid loading on the rheological, porosity distribution, optical and the microstructural properties of YAG transparent ceramic. *Ceram. Int.* **2018**, *44*, 12098–12105. [[CrossRef](#)]
10. Smith, N.A.; Mackenzie, M.D.; Morris, J.M.; Kar, A.K.; Bookey, H.T. Nd:YAG laser rod manufactured by femtosecond laser-induced chemical etching. *Opt. Mater. Express* **2021**, *11*, 3946. [[CrossRef](#)]
11. Wang, L.; Zhao, F.; Zhang, M.; Hou, T.; Li, Z.; Pan, C.; Huang, H. Preparation and photoluminescence properties of YAG:Ce<sup>3+</sup> phosphors by a series of amines assisted co-precipitation method. *J. Alloy. Compd.* **2016**, *661*, 148–154. [[CrossRef](#)]
12. Kosyanov, D.; Yavetskiy, R.P.; Tolmachev, A.; Vornovskikh, A.; Pogodaev, A.; Gridasova, E.; Shichalin, O.; Kaidalova, T.; Kuryavyi, V. Fabrication of highly-doped Nd<sup>3+</sup>:YAG transparent ceramics by reactive SPS. *Ceram. Int.* **2018**, *44*, 23145–23149. [[CrossRef](#)]
13. Kosyanov, D.; Liu, X.; Vornovskikh, A.; Kosianova, A.; Zakharenko, A.; Zavjalov, A.; Shichalin, O.; Mayorov, V.; Kuryavyi, V.; Qian, X.; et al. Al<sub>2</sub>O<sub>3</sub>-Ce:YAG and Al<sub>2</sub>O<sub>3</sub>-Ce:(Y,Gd)AG composite ceramics for high brightness lighting: Effect of microstructure. *Mater. Charact.* **2021**, *172*, 110883. [[CrossRef](#)]
14. Chrétien, L.; Boulesteix, R.; Maître, A.; Sallé, C.; Reignoux, Y. Post-sintering treatment of neodymium-doped yttrium aluminum garnet (Nd:YAG) transparent ceramics. *Opt. Mater. Express* **2014**, *4*, 2166. [[CrossRef](#)]
15. Su, Y.; Xin, M.; Chen, X.; Xing, W. Effect of CAD-CAM ceramic materials on the color match of veneer restorations. *J. Prosthet. Dent.* **2021**, *126*, 255.e1–255.e7. [[CrossRef](#)]
16. du Merac, M.R. Transparent Ceramics: Materials, Processing, Properties and Applications. In *Encyclopedia of Materials: Technical Ceramics and Glasses*; Pomeroy, M., Ed.; Elsevier: Amsterdam, The Netherlands, 2021.
17. Vorona, I.; Balabanov, A.; Dobrotvorska, M.; Yavetskiy, R.; Kryzhanovska, O.; Kravchenko, L.; Parkhomenko, S.; Mateychenko, P.; Baumer, V.; Matolínová, I. Effect of MgO doping on the structure and optical properties of YAG transparent ceramics. *J. Eur. Ceram. Soc.* **2020**, *40*, 861–866. [[CrossRef](#)]
18. Jia, W.; Su, C.; Zhang, H.; Zou, X.; Ren, G.; Wei, Q.; Zhao, M.; Ma, C. Quantitative relationship between microstructure and mechanical properties in Nd: YAG transparent ceramics. *Ceram. Int.* **2021**, *47*, 12144–12152. [[CrossRef](#)]
19. Jiang, N.; Ouynag, C.; Liu, Y.; Li, W.; Fu, Y.; Xie, T.; Liu, Q.; Pan, Y.; Li, J. Effect of air annealing on the optical properties and laser performance of Yb:YAG transparent ceramics. *Opt. Mater.* **2019**, *95*, 109203. [[CrossRef](#)]
20. Kosyanov, D.; Vornovskikh, A.; Zakharenko, A.; Gridasova, E.; Yavetskiy, R.; Dobrotvorskaya, M.; Tolmachev, A.; Shichalin, O.; Papynov, E.; Ustinov, A.; et al. Influence of sintering parameters on transparency of reactive SPSed Nd<sup>3+</sup>:YAG ceramics. *Opt. Mater.* **2021**, *112*, 110760. [[CrossRef](#)]
21. ASTM C20-00; Standard Test Methods for Apparent Porosity, Water Absorption, Apparent Specific Gravity, and Bulk Density of Burned Refractory Brick and Shapes by Boiling Water. American Society for Testing and Materials: West Conshohocken, PA, USA, 2010.
22. Golubovic, A.; Nikolic, S.; Gajic, R.; Djuric, S.; Valcic, A. The growth of Nd: YAG single crystals. *J. Serbian Chem. Soc.* **2002**, *67*, 291–300. [[CrossRef](#)]
23. Golubovic, A.; Nikolic, S.; Gajic, R.; Dohcevic-Mitrovic, Z.; Valcic, A. Growth and IR Spectra of YAG and Nd:YAG Single Crystals. *J. Metal.* **2004**, *10*, 363–370.
24. Okhupkin, M.; Skvortsov, M.; Belkin, A.; Bagayev, S. Tunable single-frequency diode-pumped Nd:YAG ring laser at 946 nm. *Opt. Commun.* **2001**, *194*, 207–211. [[CrossRef](#)]
25. Vachiramon, V.; Iamsurang, W.; Triyangkulsri, K. Q-switched double frequency Nd:YAG 532-nm nanosecond laser vs. double frequency Nd:YAG 532-nm picosecond laser for the treatment of solar lentiginos in Asians. *Lasers Med. Sci.* **2018**, *33*, 1941–1947. [[CrossRef](#)] [[PubMed](#)]

26. Yang, Y.; Xia, Z.; Guo, L.; Wu, Q.; Zhang, M.; Zeng, R.; An, Y.; Xie, Y.; Wei, W.; Ge, Y.; et al. Comparison of the efficacy and safety of a picosecond frequency-doubled 532-nm Nd: YAG Laser and a Q-switched frequency-doubled 532-nm Nd: YAG Laser for the treatment of ephelides: A randomized, split-lesion, double-center, controlled trial. *J. Cosmet. Dermatol.* **2023**, *22*, 712–714. [[CrossRef](#)] [[PubMed](#)]
27. Zhu, Y.; Yu, L.; Fu, X. Tunable continuous-wave laser operation of Nd:YAG around 1.3  $\mu\text{m}$ . *Laser Phys.* **2023**, *33*, 055004. [[CrossRef](#)]

**Disclaimer/Publisher’s Note:** The statements, opinions and data contained in all publications are solely those of the individual author(s) and contributor(s) and not of MDPI and/or the editor(s). MDPI and/or the editor(s) disclaim responsibility for any injury to people or property resulting from any ideas, methods, instructions or products referred to in the content.